Effect of power output difference on natural convection in heat pipe micro-MSR

Jiangyu Zhou,[1,2], Xingwei Chen[1,2], Ye Dai[1,2,]*

[1]*National Key Laboratory of Thorium Energy, Shanghai Institute of Applied Physics, Chinese Academy of Sciences, Shanghai 201800, China*
[2]*University of Chinese Academy of Sciences, Beijing 100049, China*
**daiye@sinap.ac.cn*

Keywords: Micro-MSR, Power output difference, Natural convection, Heat transfer

Abstract

Heat pipe molten salt reactors are well-suited for deep space and deep-sea exploration due to their compactness, safety, and efficient heat transfer. Based on a designed 50 kWt micro molten salt reactor (micro-MSR), an experimental prototype was developed to study its key technologies. The prototype differs from the conceptual reactor, necessitating numerical simulations to validate the experimental setup. This study utilizes numerical simulation methods to emulate the prototype's constant-temperature control functionality by varying thermal boundary conditions, thereby modulating the thermal power output. Through this approach, comprehensive performance data across multiple operating conditions were obtained, enabling systematic analysis of the temperature and flow field distribution characteristics within the prototype's reactor core. The simulation results validate the safety and reliability of the experimental prototype's design. Key findings include: 1) Core develops annular convection along concentric rings driven by thermal density gradients. 2) Molten salt temperature increases vertically with elevation, forming localized hotspots in the upper core region. The results provide critical theoretical references for understanding molten salt thermal-hydraulic behavior in the prototype, while offering fundamental support for subsequent experimental investigations using this test facility.

1 Introduction

Heat pipe is a highly efficient, passive heat transfer device that utilizes phase change (evaporation/condensation) and capillary action to transport thermal energy between a heat source and heat sink.

Heat pipe offers significant advantages by achieving exceptionally high thermal conductivity within limited flow cross-sections, while maintaining low pressure drop and complete isolation between the working fluid and external environment. These characteristics make it widely applicable in reactor design, as evidenced by heat pipe-cooled reactor types such as HOMER [1], Kilopower [2], and Megapower [3], which were specifically developed for space exploration missions.

Numerous researchers have attempted to integrate molten salt reactors with heat pipe technology [4], developing heat pipe-based residual heat removal systems for MSRs, or direct core cooling systems employing high-temperature heat pipes, and investigated molten salt natural convection phenomena. Wang et al. [5,6,7] demonstrated the feasibility of a heat pipe-cooled passive residual heat removal system (PRHRS) for MSRs using FLiNaK molten salt, conducted experimental investigations on its transient performance and performed numerical simulations of the natural convection characteristics. Liu et al. [8] designed an experimental system to conduct a test on the natural convection between the fluoride salt and a vertical array of heat pipes in the drain tank, the result illustrated that thermal stratification occurs in the molten salt within the vessel along the gravitational axis. Jeong et al. [9] has studied the natural convection heat transfer characteristics of molten salt with internal heat generation. The study found that external heat flux creates steep temperature gradients and thin thermal boundary layers near heater walls due to molten salt's low conductivity, whereas internal heat generation produces flatter temperature profiles from uniform heating. These distinct thermal behaviors lead to localized upward wall flows under heat flux but system-wide natural circulation under IHG.

Cui et al. [10] has made a preconceptual nuclear design of a 50 kW heat pipe cooled micro molten salt reactor (micro-MSR). The schematic diagram of the micro-MSR concept is illustrated in Fig. 1. The reactor employs molten salt as fuel and utilizes heat pipes for passive heat transfer, coupled with a thermoelectric or Stirling power conversion system at the back end. This design significantly reduces the need for molten salt pumps and valves, resulting in a compact and simplified system. Thus it demonstrates versatile applicability for deep-sea deployments, land-based nuclear power plants, and other operational scenarios.

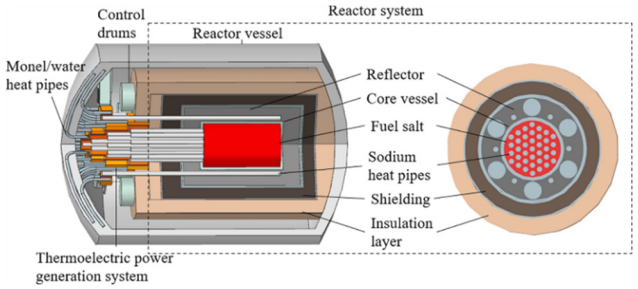

Fig. 1. Schematic diagram of the micro-MSR

Multiple researches have been conducted around this conceptual micro-MSR. Cui et al. [11,12] conducted structural optimization based on this concept reactor design and performed accident scenario analysis. The optimized design maintains a negative temperature reactivity coefficient while achieving a more compact and lightweight core, suitable for off-grid applications in space and marine environments. Liu et al. [13] use numerical simulations to study the impact of ocean conditions on the thermal-hydraulic performance. The research focuses on the influence of rolling motion on the reactor core under different ocean conditions. The results concluded that despite transient fluctuations, the reactor maintains stable performance, confirming that HP-MSRs are robust in ocean environments. Chen et al. [14] studied various core configurations with heat pipes arranged in triangular and concentric circular layouts, focusing on how different layouts, heat pipe numbers, and pipe diameters affect the reactor's temperature distribution and heat transfer performance. The results concluded that the concentric circular heat pipe configuration is identified as the optimal design for micro-MSRs, offering more uniform temperature distribution and better stability compared to the triangular layout. All the researches about the micro-MSR mentioned above remained on theoretical stage.

The operation and startup of the micro-MSR involve multiple critical technologies, including molten salt convection, heat pipe phase change, and coupled heat transfer. To validate the rationality, reliability, and accuracy of the reactor system's engineering design and manufacturing processes, based on the parameters of the micro-MSR, an experimental prototype has been developed. This prototype employs external heating to simulate nuclear heat generation from fuel salt and utilizes multiple heat pipes for heat transfer with air cooling for heat dissipation. The prototype incorporates key structural components corresponding to those of a micro-MSR, including the reactor core and the heat pipe heat transfer system. The key technical specifications are listed in Table 1.

The experimental prototype's molten salt heating mechanism differs from the uniform volumetric heat generation in actual fuel salt functioning systems, with additional variations in heat pipe configuration and arrangement. These differences prevent direct extrapolation of the prototype's thermal-hydraulic performance from theoretical reactor models. A comprehensive investigation of the startup processes—including molten salt natural convection, salt-to-heat pipe heat transfer, and internal heat pipe thermal transport—becomes essential to validate operational parameter safety, establish experimental protocols, and generate reliable performance data. Such systematic study will not only verify the coupled system's reliability but also provide crucial engineering references for heat pipe molten salt reactor design.

This study employs Fluent software to establish a three-dimensional numerical model of the experimental reactor's core-heat pipe assembly, conducting systematic simulations to analyze temperature and flow field distributions under varying heating powers in the horizontal core configuration. The results provide critical theoretical references for understanding molten salt thermal-hydraulic behavior in the prototype, while offering fundamental support for subsequent experimental investigations using this test facility.

Table 1 Main technical parameters

Parameters	Heat Pipe MSR	Prototype
Maximum Power, kW	50	75
Design Temperature, °C	800	750
Molten Salt Zone in Vessel, m	ϕ0.35 × 0.62	ϕ0.35 × 0.62
Type of Molten Salt	72.5LiF–27.5UF_4	Li_2CO_3–Na_2CO_3–K_2CO_3
Vessel Material	Hastelloy	316 Stainless Steel
Number of Heat Pipes	37	24 heat pipes + 13 heating rods
Heat Pipe Length, mm	620 + 260 + 140~440	600 + 200 + 400
Heating System	Fuel Salt	Ceramic heating belt + heating rods
Energy Utilization	Thermoelectric generation + seawater cooling	Heat exchanger + gas cooling
Insulation Material	10 cm Nano Insulation	15 cm Aluminosilicate Fiber

2. Methodology

The prototype machine is shown in Fig. 2. Its main systems include a molten salt vessel, heaters, a heat pipe array, and a heat exchanger. The molten salt vessel contains the molten salt with heating rods and heat pipes inserted internally and heating tapes wrapped externally. The heating system consists of a 13-rod heating array and externally wrapped heating tapes, which work in concert to heat the molten salt. The heat pipe array forms an annular configuration with 6 pipes in the inner ring and 18 pipes in the outer ring, transferring heat from the molten salt to the heat exchanger. In the heat exchanger, the coolant extracts heat from the heat pipes and dissipates it to the environment.

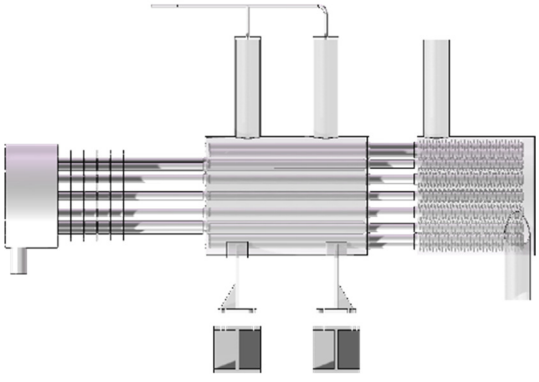

Fig. 2. 3D model of prototype

The critical aspect and overheating risk in the thermal analysis of the heat pipe MSR system lie in the core-heat pipe structure, which is therefore selected for modeling and numerical simulation.

2.1 Geometric Modeling

The molten salt vessel has an inner diameter of 350 mm, an internal height of 600 mm, and a wall thickness of 5 mm. The heat pipes extend 600 mm into the vessel. The heating rods are inserted through the core from the heating rod side, while the heat pipes are installed from the heat pipe side. All alloy components in contact with the molten salt, including the vessel, heat pipes, and heating rods, are constructed of 316 stainless steels.

The molten salt vessel is equipped with 24 high-temperature heat pipe through-holes (32 mm in diameter) arranged in two concentric circles on the heat pipe side. The inner circle consists of 6 through-holes with their centers located 50 mm from the center of the vessel, while the outer circle has 18 through-holes with centers 150 mm from the vessel center. On the heating rod side, there are 13 heating rod through-holes (32 mm in diameter) arranged in two concentric circles. The inner circle contains a single through-hole positioned at the center of the vessel, and the outer circle comprises 12 through-holes with centers 100 mm from the vessel center.

During the 3D modeling process, computational simplifications were implemented by substituting the heat pipe working mechanism with an equivalent thermal conductivity coefficient.

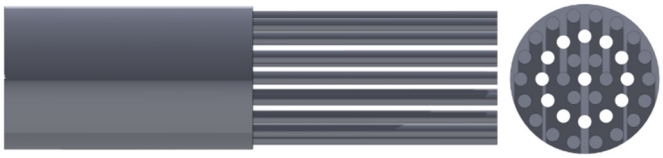

Fig. 3. Geometry model

Fig. 3 illustrates the schematic diagram of the geometric model, while Table 2 presents the relevant geometric parameters of the core-heat pipe assembly. The core is filled with alkali carbonate eutectic molten salt (32.12 wt.% Li_2CO_3 - 33.36 wt.% Na_2CO_3 - 34.52 wt.% K_2CO_3), with both the heat pipes and heating rods arranged in concentric circular configurations.

Table 2 Core–Heat Pipe Related Parameters

Geometric Parameters	Value
Core Height / mm	600
Core Diameter / mm	350
Number of Heater Rods	13
Heater Rod Diameter / mm	32
Number of Heat Pipes	24
Heat Pipe Diameter / mm	32
Array Radii / mm	150/100/50
Heat Pipe Evaporator Section Length / mm	600
Heat Pipe Adiabatic Section Length / mm	200
Heat Pipe Condenser Section Length / mm	400

2.2 Governing equations

In the present model, the heater temperature and power distribution are considered sufficiently uniform, thus radiative heat transfer is neglected. The critical Grashof number (Gr) for the transition from laminar to transitional natural convection flow is 3×10^9. In our core model, the fluid Gr number remains below 10^8, indicating laminar flow conditions. Viscous dissipation is also disregarded in this study, while the Boussinesq approximation is adopted. The governing equations for natural convection in a three-dimensional steady-state enclosed cylindrical cavity are as follows:

Continuity Equation:

$$\frac{\partial u}{\partial x}+\frac{\partial v}{\partial y}+\frac{\partial w}{\partial z}=0 \tag{1}$$

Momentum Equation:

$$u\frac{\partial u}{\partial x}+v\frac{\partial v}{\partial y}+w\frac{\partial w}{\partial z}=-\frac{1}{\rho}\frac{\partial p}{\partial x}+\nu\nabla^2 u \tag{2}$$

$$u\frac{\partial u}{\partial x}+v\frac{\partial v}{\partial y}+w\frac{\partial w}{\partial z}=-\frac{1}{\rho}\frac{\partial p}{\partial y}+\nu\nabla^2 v+g\alpha_v(T_w^{eva}-T_{salt}) \tag{3}$$

$$u\frac{\partial u}{\partial x}+v\frac{\partial v}{\partial y}+w\frac{\partial w}{\partial z}=-\frac{1}{\rho}\frac{\partial p}{\partial z}+\nu\nabla^2 w \tag{4}$$

Energy Equation:

$$u\frac{\partial T}{\partial x}+v\frac{\partial T}{\partial y}+w\frac{\partial T}{\partial z}=a\nabla^2 T+S \tag{5}$$

Where u, v, w represent velocities on x, y, z directions, m/s, ρ is the density of molten salt, kg/m^3, p is the pressure, Pa, ν is the kinematic viscosity, m^2/s, g is the acceleration of gravity, m/s^2, α_v is the coefficient of thermal expansion, 1/K, a is the thermal diffusivity, m^2/s, T_w^{eva} is the surface temperature of heat pipe evaporator section, K, T_{salt} is the average temperature of molten salt, K. S is source term.

2.3 Boundary conditions

The heat pipes and reactor core vessel walls are treated as no-slip boundaries. The adiabatic sections of the heat pipes, along with the top and bottom surfaces of the molten salt vessel, are assumed to be adiabatic boundaries. To simplify computations, the outer wall temperature of the heat pipe condenser section is assumed to remain uniform and constant, serving as the ultimate heat sink. The operational mechanism of the heat pipes is represented through an equivalent thermal conductivity coefficient.

Due to the temperature control system integrated into the prototype's heating program, the heating module is set to maintain a constant temperature of 923.15 K. The total heat transfer of the system is regulated by adjusting the wall temperature of the heat pipe condenser section. In this study, the outer wall temperatures of the heat pipe condenser section are specifically set at 673.15 K, 723.15 K, 773.15 K, 823.15 K, and 873.15 K, respectively.

2.4 Material properties

The conceptual heat pipe molten salt reactor corresponding to the prototype employs FLiU fuel salt, which was primarily selected based on neutron physics considerations. However, the use of fluoride salts presents significant challenges in experimental prototypes due to their high cost and stringent operational requirements. In contrast, ternary Li_2CO_3-Na_2CO_3-K_2CO_3 carbonate salts offer distinct advantages for physical mechanism investigations, such as natural convection studies, owing to their relatively low melting points and high operating temperatures. Consequently, the molten salt vessel in the prototype is filled with Li_2CO_3-Na_2CO_3-K_2CO_3. The relevant physical properties [15] are summarized in Table 3.

Table 3 Physical Parameters of Molten Salt

Parameters	Value
Salt combination	32.12 wt.% Li_2CO_3 - 33.36 wt.% Na_2CO_3 - 34.52 wt.% K_2CO_3
Melting Point / K	669.95
Maximum Operating Temperature / K	1067.15
Density / g/cm³	2.27 - 4.34 × 10^{-4}T
Viscosity / mPa·s	0.0852 × exp(3.51 × 10^{-4}/RT)
Specific Heat / J/(g·K)	1.612
Thermal Conductivity / W/(m·K)	0.499

2.5 Heat transfer parameters

The average convective heat transfer coefficient h_{ave} at the evaporator section surface of the heat pipe is calculated using Newton's law of cooling:

$$h_{ave} = \frac{q_{ave}}{T_{w,ave}^{eva} - T_{salt}} \tag{6}$$

Where q_{ave} is the average surface heat flux density of the heat pipe evaporator section, W/m^2, $T_{w,ave}^{eva}$ is the average surface temperature of the heat pipe evaporator section, K.

The average Nusselt number Nu_{ave} for natural convection heat transfer at the evaporator section surface of the heat pipe is calculated by the following expression:

$$Nu_{ave} = \frac{h_{ave}L}{\lambda} \tag{7}$$

Where L is the characteristic length of the heat pipe, m, λ is the thermal conductivity of molten salt, W/(m·K).

2.6 Numerical procedures

The governing equations are numerically solved using the commercial CFD package of ANSYS Fluent. The geometric model is constructed in Design Modeler, and the steady-state, pressure-based solver is employed to solve the governing equations. The Coupled algorithm is adopted for pressure-velocity coupling, while the PRESTO! scheme is utilized for pressure discretization. The convective terms in the momentum and energy equations are discretized using a second-order upwind differencing scheme to enhance numerical accuracy while maintaining solution stability.

Additionally, the heat flux at the condenser wall surface and the net system heat flux are monitored throughout the simulation. Iterative calculations continue until convergence is achieved, evidenced by stabilized residual curves, asymptotic stabilization of the condenser wall heat flux, and the net system heat flux approaching zero within an acceptable tolerance, all verified through monitoring point data consistency.

2.7 Grid distributions and grid independence test

During the meshing process, a surface mesh dominated by quadrilateral elements is initially generated, with boundary layers added near the wall surfaces. To resolve the thermal and flow boundary layers that diminish in thickness with increasing distance from the wall, the mesh density is progressively refined closer to the walls. This surface mesh is then extruded to form a volume mesh primarily composed of hexahedral elements. The resulting mesh configuration is illustrated in Fig. 4.

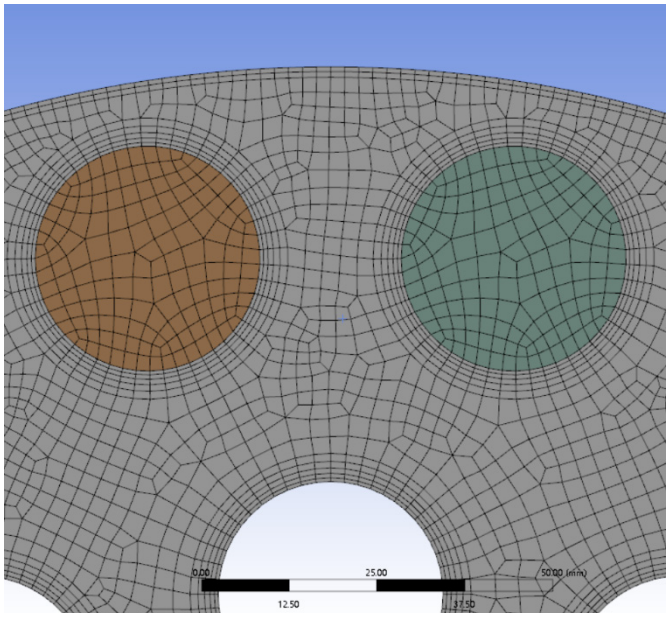

Fig. 4. Grid distribution details

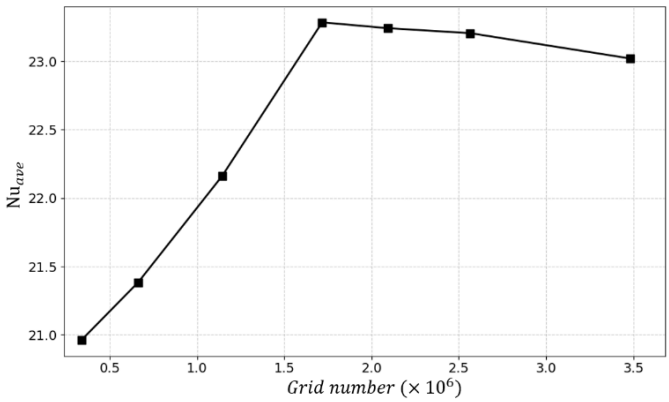

Fig. 5. Grid Independence

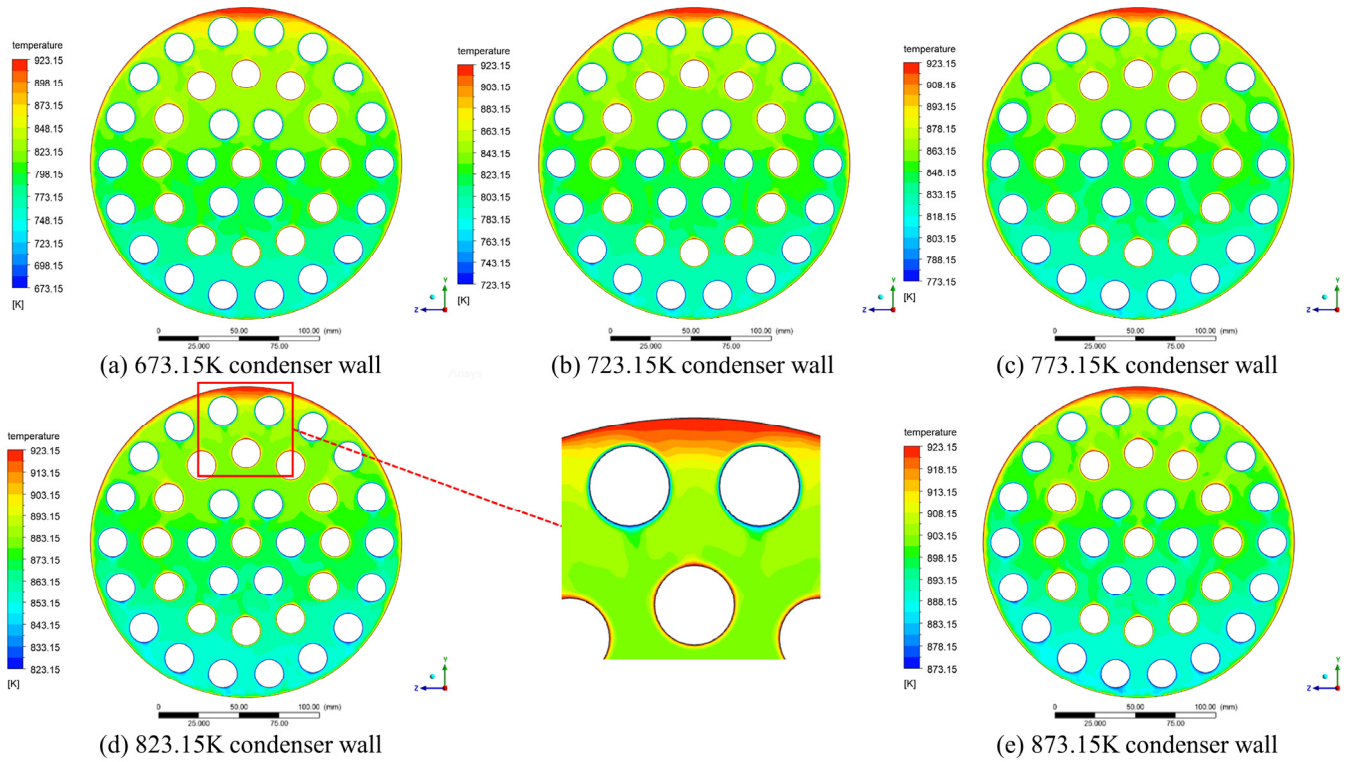

(a) 673.15K condenser wall (b) 723.15K condenser wall (c) 773.15K condenser wall

(d) 823.15K condenser wall (e) 873.15K condenser wall

Fig. 6. Contours of temperature in reactor cores with different condenser wall conditions

To eliminate grid dependence and ensure solution reliability, a grid independence study was conducted to balance solution accuracy with computational cost. Fig. 5. presents the grid independence verification for the model with the heating module maintained at a constant 923.15 K and the heat pipe condenser wall fixed at 823.15 K. The variation in the average Nusselt number exhibits an increasing trend as the grid count increases. When the grid count reaches approximately 2×10^6, the changes in the average Nusselt number become negligible. To balance computational accuracy and cost, a mesh configuration with 2,092,000 cells was ultimately adopted.

3 Results

3.1 Analysis of temperature fields across operating conditions

To better visualize the core fluid dynamics in post-processing results, the heat pipe structural visibility was intentionally disabled in all graphical outputs presented in this study. Fig. 6. displays the core temperature field and velocity distribution under the condition of a fixed heating module temperature at 923.15 K. The temperature contour results demonstrate that the natural convection flow direction aligns with gravity in all operational cases. The primary temperature gradient develops along the y-axis, exhibiting increasing molten salt temperatures with elevation. Thermal hotspots are predominantly concentrated in the upper core region. This phenomenon arises from inherent design limitations of the horizontal core configuration, where the non-uniform distribution of heat pipes along the gravitational direction creates suboptimal heat transfer efficiency, particularly at the uppermost core region.

Notably, the molten salt exhibits higher temperatures near the heating rods and vessel walls, while lower temperatures prevail next to the condenser sections of the heat pipes. Non-uniform thermal stratification develops at all wall interfaces due to buoyancy-driven convection under gravity. Specifically, the heated salt expands along high-temperature surfaces (heating rods and vessel walls), reducing its density and inducing upward flow. Conversely, heat rejection at the evaporator sections causes salt contraction and downward flow due to increased density. The thermal stratification intensifies proportionally with the temperature differential between the heating module and heat pipe evaporator walls.

3.2 Analysis of flow fields across operating conditions

Fig. 7 presents the velocity vector field on the reactor core's cross-section. It reveals that upward molten salt flow occurs near the heated surfaces (heating rods and vessel walls) due to their heating process, while downward flow occurs near the heat pipe evaporator sections due to cooling effects. While variations in the condenser wall temperature show limited influence on the overall flow pattern distribution, they primarily affect the magnitude of molten salt velocities. Enhanced temperature differentials proportionally increase flow velocities, thereby intensifying natural convection heat transfer within the system.

Fig. 7 also reveals significantly higher flow velocities mainly distributed along the lateral regions of the cross-section, while the central zone maintains relatively moderate flow rates. This flow distribution pattern stems from the reduced circumferential curvature of heat pipe/heating rod arrays in lateral areas compared to the central region. The diminished curvature facilitates vertically aligned single-column arrays

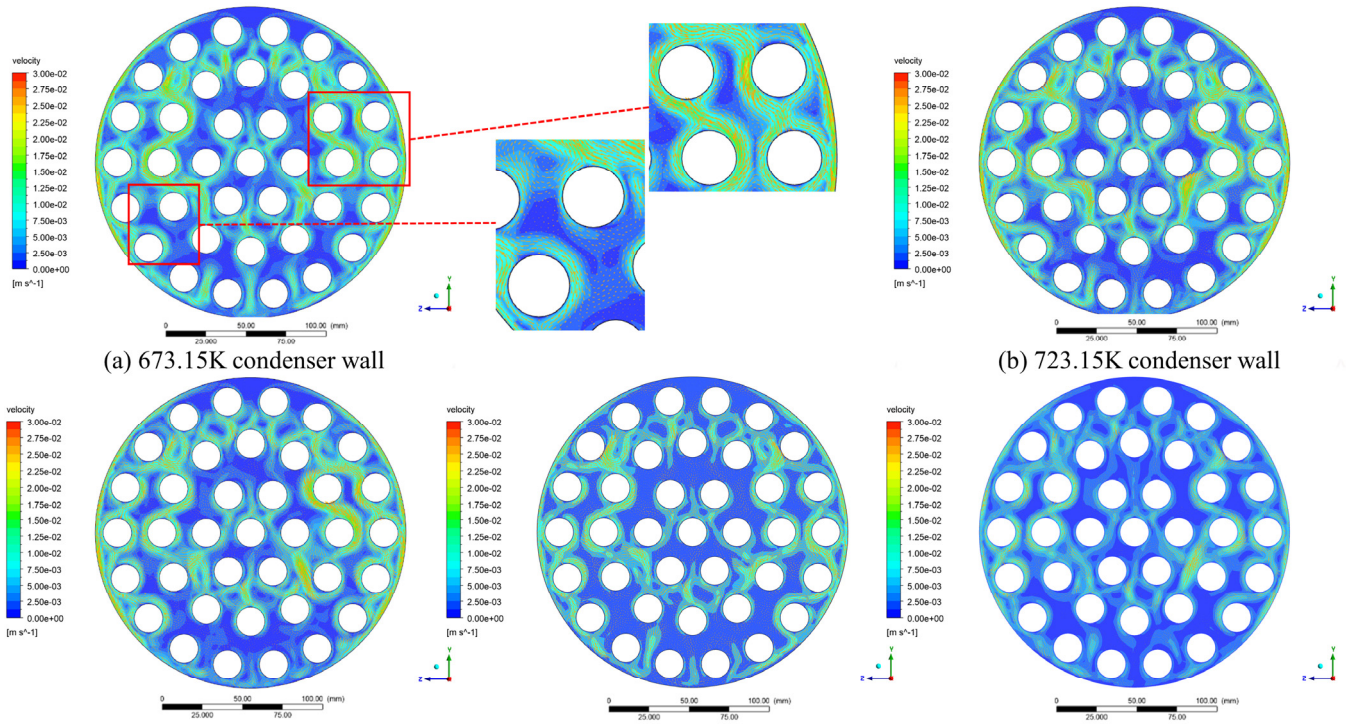

(a) 673.15K condenser wall (b) 723.15K condenser wall

(c) 773.15K condenser wall (d) 823.15K condenser wall (e) 873.15K condenser wall

Fig. 7. Velocity vector of reactor cores with different condenser wall conditions

which contain only heat pipes or heating rods, enabling sustained unidirectional thermal effects (either continuous heating or cooling) that propel molten salt toward the vessel's top or bottom with minimal flow interference. Correspondingly, the inner regions exhibit vertically stacked heat pipe-heating rod arrays, subjecting the molten salt to counteracting thermal effects—ascending flows encountering cooling or descending flows reheating. These opposing interactions weaken flow momentum, manifesting as reduced velocities and degraded fluidity compared to lateral zones. This velocity attenuation phenomenon is similarly observed at the stacked annular arrays of outer-circle heat pipes and heating rods, as evidenced in the extended view of Fig. 7 (a).

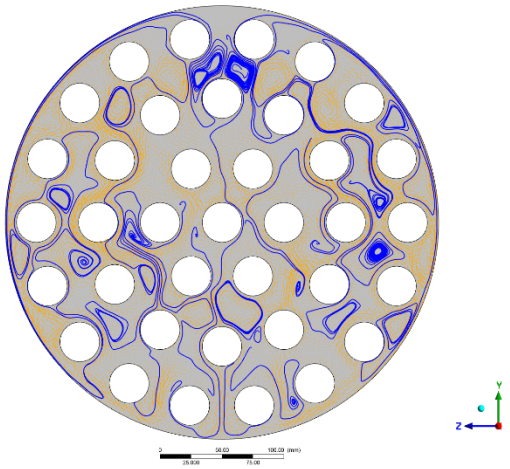

Fig. 8. Fluid flow streamline distribution in reactor core

Fig. 8 illustrates the streamline distribution within the reactor core cross-section under the condition of a constant 673.15 K heat pipe condenser wall temperature. The visualization reveals distinct vortex formation at flow convergence zones where ascending and descending flows interact. Along the vessel walls, the molten salt exhibits unidirectional upward flow driven by heating, ultimately developing stagnation regions at the upper core region. This is a phenomenon that correlates directly with the observed localized hotspot formation.

3.3 Analysis of thermal power across operating conditions

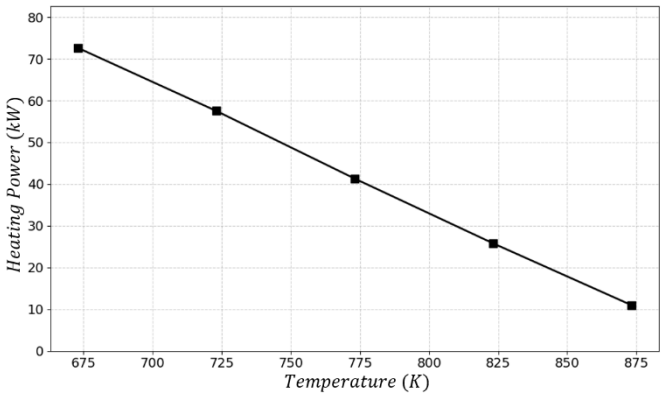

Fig. 9. Heating power under different condenser wall temperature

As shown in Fig. 9, the system thermal power varies under different operating conditions. With the heating module temperature fixed at 923.15 K, the core molten salt average temperature increases while the system thermal power

decreases as the set temperature of the heat pipe condenser wall rises. The maximum thermal power occurs in the case with the heat pipe condenser wall temperature set at 673.15 K, which is 72.6kW. Under constant heating temperature conditions, lower condenser wall temperatures result in greater system heat dissipation capacity and consequently higher system thermal power. This demonstrates that enhanced cooling capacity at the heat pipe cold end directly enables higher system power dissipation requirements.

4 Conclusion

This study systematically investigates the natural convection characteristics and thermal performance of an experimental prototype designed based on specific heat pipe molten salt reactor parameters under varying power distributions through numerical simulations. The main findings are summarized as follows:

1) The core forms annular natural convection flows along the inner and outer rings of the concentric array, and the core natural convection is driven by thermally induced density gradients.

2) Molten salt temperatures increase vertically along the elevation. Localized hotspots predominantly form in the upper core region due to flow stagnation.

In addition to steady-state operation under constant temperatures, the natural convection heat transfer characteristics of molten salt in the experimental prototype must be thoroughly investigated during transient conditions such as startup& shutdown, temperature variations, and thermal runaway scenarios. Consequently, follow-up studies will incorporate factors like power fluctuations and full-load transients to analyze their impacts on molten salt convection through temperature/flow field evolution.

5 Acknowledgements

This work is supported by Fundamental Research Program of Industrial Foundation (No. SINAP-CYJJ-202503).

6 References

[1] Poston D I. The heatpipe-operated Mars exploration reactor (HOMER) [C]//AIP Conference Proceedings. American Institute of Physics, 2001, 552(1): 797-804.

[2] McClure P R, Poston D I, Dixon D D. Final results of Demonstration Using Flattop Fissions (DUFF) experiment [R]. Los Alamos National Lab.(LANL), Los Alamos, NM (United States), 2012.

[3] McClure P R, Reid R S, Dixon D D. Advantages and applications of megawatt sized heat pipe reactors [R]. Los Alamos National Laboratory (LANL), Los Alamos, NM (United States), 2012.

[4] Roper R, Harkema M, Sabharwall P, et al. Molten salt for advanced energy applications: A review [J]. Annals of Nuclear Energy, 2022, 169: 108924.

[5] Wang C, Guo Z, Zhang D, et al. Transient behavior of the sodium–potassium alloy heat pipe in passive residual heat removal system of molten salt reactor [J]. Progress in Nuclear Energy, 2013, 68: 142-152.

[6] Wang C, Liu M, Zhang D, et al. Experimental study on transient performance of heat pipe-cooled passive residual heat removal system of a molten salt reactor [J]. Progress in Nuclear Energy, 2020, 118: 103113.

[7] Wang C L, Qin H, Zhang D L, et al. Numerical investigation of natural convection characteristics of a heat pipe-cooled passive residual heat removal system for molten salt reactors [J]. Nuclear Science and Techniques, 2020, 31(7): 65.

[8] Liu M, Zhang D, Wang C, et al. Experimental study on heat transfer performance between fluoride salt and heat pipes in the new conceptual passive residual heat removal system of molten salt reactor [J]. Nuclear Engineering and Design, 2018, 339: 215-224.

[9] Jeong Y S, Seo S B, Bang I C. Natural convection heat transfer characteristics of molten salt with internal heat generation [J]. International Journal of Thermal Sciences, 2018, 129: 181-192.

[10] Cui D Y, Dai Y, Cai X Z, et al. Preconceptual nuclear design of a 50 kWth heat pipe cooled micro molten salt reactor (micro-MSR) [J]. Progress in Nuclear Energy, 2021, 134: 103670.

[11] Cui D Y, Li X X, Dai Y, et al. An improved core design of a 50 kWth heat pipe cooled micro Molten Salt Reactor (micro-MSR) [J]. Progress in Nuclear Energy, 2022, 151: 104326.

[12] Cui D Y, Li X X, Dai Y, et al. Accident scenario analysis and control scheme design for a micro Molten Salt Reactor [J]. Progress in Nuclear Energy, 2024, 172: 105208.

[13] Liu Z, Liu L, Guo Z, et al. Numerical simulation of the ocean conditions impact on heat pipe-cooled molten salt reactor core thermal-hydraulic performance [J]. Nuclear Engineering and Design, 2024, 421: 113066.

[14] Chen X, Zou Y, Chen Z, et al. Effect of core configuration on natural convection and heat transfer in heat pipe cooled micro-MSRs [J]. Nuclear Engineering and Design, 2022, 395: 111839.

[15] An X, Cheng J, Zhang P, et al. Determination and evaluation of the thermophysical properties of an alkali carbonate eutectic molten salt [J]. Faraday discussions, 2016, 190: 327-338.